Supramolecular Chemistry
Publication details, including instructions for authors and subscription information:
http://www.informaworld.com/smpp/title~content=t713649759

A Macrocyclic Effect on the Reduction of *p*-Quinones

Hirohiko Houjou[a]; Sung-Kil Lee[a]; Yoshinobu Nagawa[a]; Kazuhisa Hiratani[a]
[a] Nanoarchitectonics Research Center, National Institute of Advanced Industrial Science and Technology (AIST), Tsukuba, Ibaraki, Japan

To cite this Article Houjou, Hirohiko , Lee, Sung-Kil , Nagawa, Yoshinobu and Hiratani, Kazuhisa(2001) 'A Macrocyclic Effect on the Reduction of *p*-Quinones', Supramolecular Chemistry, 13: 6, 683 — 692
To link to this Article: DOI: 10.1080/10610270108027498
URL: http://dx.doi.org/10.1080/10610270108027498

Supramolecular Chemistry, Vol. 13, pp. 683–692
Reprints available directly from the publisher
Photocopying permitted by license only

A Macrocyclic Effect on the Reduction of *p*-Quinones

HIROHIKO HOUJOU, SUNG-KIL LEE, YOSHINOBU NAGAWA and KAZUHISA HIRATANI*

Nanoarchitectonics Research Center, National Institute of Advanced Industrial Science and Technology (AIST), 1-1-1 Higashi, Tsukuba, Ibaraki 305-8562, Japan

A macrocyclic compound that has four phenolic and four aromatic amino groups is synthesized. This compound reacts with *p*-quinones to give regiospecific oxidation products. During the reaction, the quinone is reduced to its hydroquinone form. The rate constant for the macrocycle is significantly large compared to its acyclic analogues. Analysis of the rate constants for several *p*-quinones indicates that the rate determining step involves an electron transfer process. Cyclic voltammetry measurement suggests that the complexation of the macrocycle with the quinone is related to lowering of the activation barrier of electron transfer. The role of the phenolic groups in the complexation is discussed. Based on the experimental results, the macrocyclic effect is evaluated to be 27 kJ mol^{-1} as the difference in Gibbs energy change necessary for the complexation.

Keywords: Macrocycic effect; Redox reaction; *p*-Quinones; Molecular recognition

INTRODUCTION

Redox reactions of *p*-quinones have attracted much attention not only for their biological importance but also from the viewpoint of the construction of intelligent molecular systems for a specific function such as electron transfer or energy transfer [1–3]. The mechanism of the reduction of quinones by NADH analogue or other artificial reductant has been extensively studied [4–8]. In most of the cases the reaction is initiated with a one-electron transfer, which is usually an endergonic process, and hence is the rate determining step. The following rapid processes include H^+, e^-, and H^+ transfers, and their sequence depends on the system.

Since an efficient electron transfer can occur only when the electron donor (D) and acceptor (A) sufficiently approach each other, the charge-transfer (CT) complex has been implicated as the prerequisite intermediate in this process. In fact, it is known that CT complexes play an important role when the heat of formation of the complex is so small that the apparent activation energy could be negative [9]. On the other hand, it has also been reported that protons or some metal ions show catalytic action by stabilizing the reduced state of A [10]. For example, the one electron reduction potential of *p*-benzoquinone (A) appreciably shifts in the positive direction

*Corresponding author.

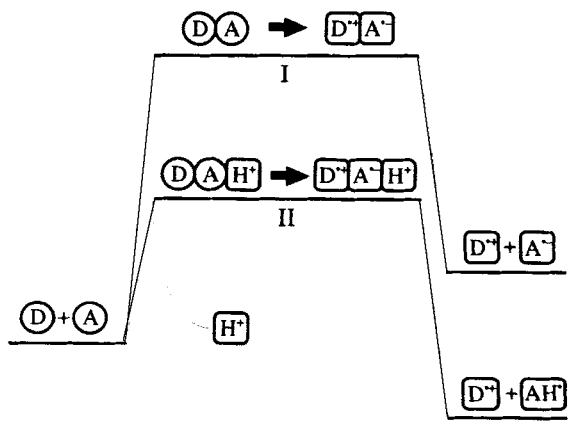

FIGURE 1 Schematic representation of an electron transfer reaction from a donor (D) to an acceptor (A). If the reduced state of A is stabilized by a proton, it can serve as a catalyst: the activation energy in the presence of proton (II) is decreased compared with that in the absence of proton (I).

with a decrease of pH in the region of pH < pK_1, where K_1 is the dissociation constant of protonated semiquinone ($AH^{\cdot}$) [5]. It is unfavorable for *p*-benzoquinone to associate with a proton in its neutral state, since its basicity is quite low (pK = −7) [11]. This implies that a necessary condition for catalytic action is interaction with a substrate in its transition state. In other words, it is unnecessary that a catalyst has affinity to a substrate in its initial state. This can be schematically shown in Fig. 1 [10].

If higher performance in molecular system using the redox reaction of quinones is to be achieved, then a more precise molecular design is needed. There have been several supramolecular systems that were designed so as to realize an efficient electron transfer [2,3,12,13]. In these systems, the porphyrin unit is utilized as an electron donor. In terms of molecular recognition, it is well known that a macrocyclic structure gives rise to a drastic improvement, so-called "macrocyclic effect", in performance such as reactivity, selectivity, stability, and so on [14,15]. Thus, it is expected that an electron donor compound having a macrocyclic structure shows prominent reduction ability or substrate specificity. As far as we know, however, there has been no reported macrocyclic quinone receptors which act as electron donors.

Quite recently we have synthesized a novel macrocyclic compound (**1**) that has plural OH groups on its ring frame by a simple and efficient synthetic method [16]. We have found that the ability to reduce *p*-quinones to hydroquinones (during the reaction, **1** is oxidized into **2** and **3**). In view of the reaction rate, **1** shows appreciably high ability of reducing quinones in comparison with its acyclic analogues **4a**–**e**. In this paper, we will show how the OH groups of **1** play an important role in the reaction, and how the macrocyclic structure affects the reaction rate.

MATERIALS AND METHODS

Tetramine **1** was synthesized according to the reported procedure [16]. Acyclic analogues **4a**–**e** were prepared from the corresponding phenylenediamine and hydroxybenzaldehydes. A typical procedure was as follows: 2.44 g of salicylaldehyde was added to a methanol solution of *p*-phenylenediamine (1.08 g/100 ml), resulting in an orange precipitate of disalicylidene-*p*-phenylenediamine (yield ~ quant.). This

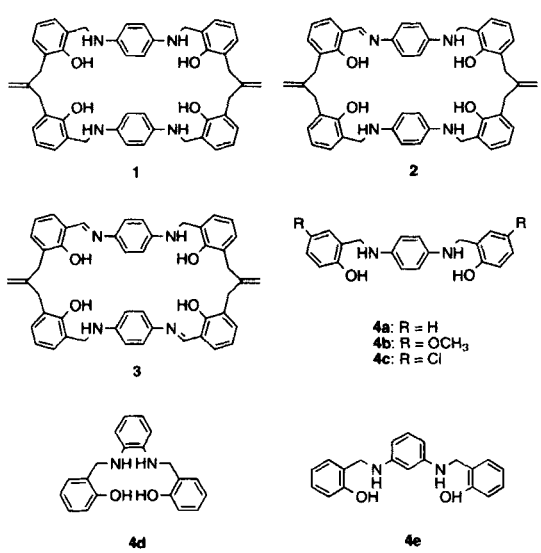

CHART 1

was reduced to **4a** by using sodium borohydride in a mixed solution of THF (60 ml) and methanol (10 ml) (yield 94%). All the products were purified by recrystalization from a chloroform–methanol mixture (1:4). Analytical data of **4a**: ^{1}H NMR (500 MHz, DMSO-d_6): δ 4.07 (*d* (4.3 Hz), Ar–CH_2–NH–, 4H), 5.15 (br.,–NH–, 2H), 6.42 (*s*, *p*-C_6H_4, 4H), 6.70 (*t*(7.3 Hz), Ar–CH_2–, 2H), 6.77 (*d*(7.9 Hz), Ar–CH_2–, 2H), 7.01 (*t*(7.0 Hz), Ar–CH_2–, 2H), 7.17 (*d*(7.1 Hz), Ar–CH_2–, 2H), 9.50 (br., –OH–, 2H). ^{13}C NMR (126 MHz, DMSO-d_6) δ 43.0, 114.0, 114.8, 118.7, 126.2, 127.3, 128.3, 140.3, 155.1. Precise MS (EI, positive mode) *m*/*z* calcd. for $C_{20}H_{20}N_2O_2$ 320.1523, found 320.1522, UV–Vis: λ_{max} = 257 nm (ε = 19000), m.p. 181°C, IR:3253, 1256, 818 cm^{-1}. **4b**: ^{1}H NMR (500 MHz, DMSO-d_6): δ 3.60 (*s*, $-OCH_3$, 6H), 4.05 (*d*(5.2 Hz), Ar–CH_2–NH–, 4H), 5.17 (br., –NH–, 2H), 6.42 (*s*, *p*-C_6H_4, 4H), 6.59 (*dd*(3.1, 8.6 Hz), Ar–CH_2–, 2H), 6.68 (*d*(8.9 Hz), Ar–CH_2–, 2H), 6.78 (*d*(3.1 Hz), Ar–CH_2–, 2H), 9.03 (br., –OH–, 2H). ^{13}C NMR (126 MHz, DMSO-d_6) δ 43.0, 55.2, 111.8, 114.0, 114.2, 115.2, 127.3, 140.2, 148.8, 152.1. Precise MS *m*/*z* calcd. for $C_{22}H_{24}N_2O_4$ 380.1735, found 380.1648, UV–Vis:λ_{max} = 255 nm (ϵ = 23000), m.p. 189–191°C, IR:3266, 1223, 1048 cm^{-1}. **4c**: ^{1}H NMR (500 MHz, DMSO-d_6): δ 4.07 (*s*, Ar–CH_2–NH–, 4H), 5.32 (br., –NH–, 2H), 6.40 (*s*, *p*-C_6H_4, 4H), 6.78 (*d*(8.5 Hz), Ar–CH_2–, 2H), 7.04 (*dd*(2.5, 8.6 Hz), Ar–CH_2–, 2H), 7.17 (*d*(2.5 Hz), Ar–CH_2–, 2H), 9.81 (br., –OH–, 2H). ^{13}C NMR (126 MHz, DMSO-d_6) δ 42.2, 113.8, 116.3, 122.4, 126.8, 127.5, 128.9, 140.0, 153.9. Precise MS *m*/*z* calcd. for $C_{20}H_{18}N_2O_2Cl_2$ 388.0744, found 388.0703, UV–Vis:λ_{max} = 232 nm (ϵ = 39000), m.p. 228–232°C, IR:3261, 1262, 824 cm^{-1}. **4d**: ^{1}H NMR (500 MHz, DMSO-d_6): δ 4.23 (*d* (4.9 Hz), Ar–CH_2–NH–, 4H), 5.04 (br., –NH–, 2H), 6.42 (mult., *o*-C_6H_4, 4H), 6.73 (*t*(7.3 Hz), Ar–CH_2–, 2H), 6.81 (*d*(7.9 Hz), Ar–CH_2–, 2H), 7.04 (*t*(7.0 Hz), Ar–CH_2–, 2H), 7.20 (*d*(7.4 Hz), Ar–CH_2–, 2H), 9.54 (br., –OH–, 2H). ^{13}C NMR (126 MHz, DMSO-d_6) δ 42.2, 110.0, 114.8, 117.2, 118.7, 125.7, 127.5, 128.4, 136.1, 155.1. Precise MS *m*/*z* calcd. for $C_{20}H_{20}N_2O_2$ 320.1523, found 320.1537, UV–Vis: λ_{max} = 226 nm (ϵ = 19000), m.p. 113–116°C, IR:3289, 1238, 749 cm^{-1}. **4e**: ^{1}H NMR (500 MHz, DMSO-d_6): δ 4.09 (*d* (6.1 Hz), Ar–CH_2–NH–, 4H), 5.57 (*t* (6.0 Hz), –NH–, 2H), 5.58 (*d*(8.0 Hz), *m*-C_6H_4, 2H), 5.89 (*s*,*m*-C_6H_4, 1H), 6.69 (*t*(7.9 Hz), *m*-C_6H_4, 1H), 6.70 (*t*(7.3 Hz), Ar–CH_2–, 2H), 6.78 (*d*(7.9 Hz), Ar–CH_2–, 2H), 7.01 (*t*(7.6 Hz), Ar–CH_2–, 2H), 7.15 (*d*(7.3 Hz), Ar–CH_2–, 2H), 9.41 (*s*, –OH–, 2H). ^{13}C NMR (126 MHz, DMSO-d_6) δ 41.6, 96.4, 101.3, 114.7, 118.7, 126.2, 127.2, 128.2, 129.1, 149.6, 155.9. Precise MS *m*/*z* calcd. for $C_{20}H_{20}N_2O_2$ 320.1523, found 320.1536, UV–Vis:λ_{max} = 228 nm (ϵ = 28000), m.p. 125–126°C, IR:3266, 1247, 759 cm^{-1}.

In a degassed dry THF solution, **1** (1.0 mM) was allowed to react with 0.00, 0.25, 0.50, 0.75, 1.00, 1.25, 1.50, 1.75, and 2.00 equivalents of *p*-benzoquinone. After 40h, the THF was removed by evaporation. The residue was dissolved in DMSO-d_6, and its composition was determined by ^{1}H NMR spectra. The oxidation products (**2** and **3**) were isolated by silica gel (40–60 μm) column chromatography using an *n*-hexane–ethylacetate mixture (6:4) as eluant. The ^{1}H NMR signals were assigned from COSY, NOESY, and HMQC measurements, using a Brucker AVANCE500 (500 MHz for ^{1}H nuclei) system. TMS was used as an internal standard. Analytical data of **1**: ^{13}C NMR (126 MHz, DMSO-d_6) δ 35.6, 45.5, 111.8, 115.1, 119.0, 125.5, 126.0, 126.0, 128.5, 140.3, 147.2, 153.7, UV–Vis:λ_{max} = 254 nm (ϵ = 27000), m.p. 165–178°C, IR: 3314, 1620, 754 cm^{-1}. **2**: ^{1}H NMR (500 MHz, DMSO-d_6): δ 3.30 (*s*, Ar–CH_2–C(=CH_2)–, 1H), 3.34 (*s*, Ar–CH_2–C(=CH_2)–, 1H), 3.40 (*s*, Ar–CH_2–C(=CH_2)–, 1H), 3.43 (*s*, Ar–CH_2–C(=CH_2)–, 1H), 4.14 (*d*(3.8 Hz), Ar–CH_2–NH–, 1H), 4.17 (*s*, Ar–CH_2–NH–, 1H), 4.30 (*d*(5.7 Hz), Ar–CH_2–NH–, 1H), 4.52 (*s*, –C(=CH_2)–, 1H), 4.61 (*s*, –C(=CH_2)–, 1H), 4.67 (*s*, –C(=CH_2)–, 1H), 4.70 (*s*, –C(=CH_2)–, 1H), 5.49 (br., –NH–, 2H), 6.46 (*s*, *p*-C_6H_4, 4H), 6.54 (*d*(8.7 Hz), *p*-C_6H_4, 2H), 6.64–70 (mult., –CH_2–Ar–CH_2–, 2H), 6.64–70

(mult., -NH-, 1H), 6.72(*t*(7.6 Hz),-CH_2-Ar-CH_2-, 1H), 6.84 (*d*(6.0 Hz), -CH_2-Ar-CH_2-, 1H), 6.87 (*t*(7.6 Hz),-CH_2-Ar-CH_2-, 1H), 6.91 (*d*(7.3 Hz),-CH_2-Ar-CH_2-, 2H), 6.99 (*d*(6.8 Hz),-CH_2-Ar-CH_2-, 1H), 7.02 (*d*(7.7 Hz),-CH_2-Ar-CH_2-, 1H), 7.08 (*d*(7.9 Hz),-CH_2-Ar-CH_2-, 1H), 7.18 (*d*(8.9 Hz), *p*-C_6H_4, 2H), 7.20 (*d*,-CH_2-Ar-CH_2-, 1H), 7.36 (*d*(6.1 Hz),-CH_2-Ar-CH_2-, 1H), 8.80 (*s*, Ar-CH=N-, 1H), 8.8 (br., -Ar(OH)-CH_2-NH-, 1H), 9.09 (br., -Ar(OH)-CH_2-NH-, 1H), 14.09 (*s*, -Ar(OH)-CH=N-, 1H). ^{13}C NMR (126 MHz, DMSO-d_6) δ 34.9, 35.3, 35.5, 36.3, 41.4, 45.5, 111.5, 112.0, 112.8, 115.1, 115.1, 118.3, 118.9, 119.0, 119.5, 122.3, 125.6, 125.8, 125.9, 126.0, 126.5, 126.7, 128.3, 128.4, 128.8, 130.0, 132.5, 135.5, 140.3, 147.2, 147.3, 148.1, 152.7, 153.6, 153.7. FAB MS (positive mode) *m/z* 742. UV-Vis: λ_{max} = 379 nm (ϵ = 18000), m.p. 191-197°C, IR: 3421, 1617, 753 cm^{-1}. **3**: ^{1}H NMR (500 MHz, DMSO-d_6): δ 3.32 (*s*, -N=CH-Ar-CH_2-C(=CH_2)-, 4H), 3.36 (*s*, -NH-CH-Ar-CH_2-C(=CH_2)-, 4H), 4.26 (*d* (5.5 Hz), Ar-CH_2-NH-, 4H), 4.79 (*s*,-C(=CH_2)-, 2H), 4.94 (*s*, -C(=CH_2)-, 2H), 6.54 (*t*, -NH-, 2H), 6.55(*d*, *p*-C_6H_4, 4H), 6.71 (*t*(7.5 Hz), -Ar-CH_2-, 2H), 6.89(*t*, (7.5 Hz), -Ar-CH=N-, 2H), 6.93(*d* (7.3 Hz), -Ar-CH_2-NH-, 2H), 7.01 (*d*.(7.3 Hz), -Ar-CH_2-NH-, 2H), 7.22 (*d*(7.3 Hz), -Ar-CH=N-, 2H), 7.24(*d*(8.3 Hz), *p*-C_6H_4, 4H), 7.36 (*d*(7.7 Hz), -Ar-CH=N-, 2H), 8.36 (*s*, -Ar(OH)-CH_2-NH-, 2H), 8.84 (*s*, -Ar-CH=N-, 2H), 14.18 (*s*, -Ar-(OH)-CH=N-, 2H), ^{13}C NMR (126 MHz, DMSO-d_6) δ 33.9, 35.8, 41.8, 112.7, 113.4, 118.2, 118.9, 119.4, 122.4, 125.5, 126.4, 126.5, 126.7, 127.9, 129.9, 132.1, 135.4, 146.9, 148.2, 152.5, 157.2, 158.4. FAB MS (positive mode) m/s 741. Elemental Analysis calculated for $C_{48}H_{44}N_4O_4$: C, 77.81; H, 5.99; N, 7.56; found: C, 77.59; H, 6.03; N, 7.51. UV-Vis: λ_{max} = 376 nm (ϵ = 42000), m.p. 191-198°C, IR: 3437, 1616, 751 cm^{-1}.

UV-Vis measurements were carried out by using a JASCO V570 spectrometer. Samples were prepared as solutions of 1×10^{-5} -1×10^{-3} M so that the reaction rate could be appropriately determined. For solvent, a THF (for spectroscopy; KANTO Chemical) was used after degassing and N_2-substitution. All experiments were done at 25°C.

Electrochemical measurements were performed by using a conventional three-electrode cell, with PFCT carbon working electrode, platinum wire counter electrode, and Ag^+/Ag reference electrode. The samples were prepared as 1.0 mM solutions in THF (for spectroscopy; KANTO Chemical) with 0.1 M tetrabutylammonium perchlorate as supporting electrolyte. Cyclic voltammograms were run by using a BAS100B/W(CV-50W) electrochemical workstation. Solutions were purged with nitrogen to remove oxygen, and nitrogen was passed over the solution during the measurement. Values of half wave potential ($E_{1/2}$) were approximated by the average of anodic and cathodic peak potentials. Sweep rate was 100 m V/s, and its initial direction was changed depending on the sample. All these measurements were done at 20°C. Redox potential values are herein written as measured from that of Ag^+/Ag unless otherwise noted.

Melting points for **4a**, **4b**, and **4e** were measured by a conventional melting point apparatus. Melting points for **1**, **2**, **3**, **4c**, and **4d** were measured by a differential scanning calorimetry at a heating rate of 5 K/min, and were shown as a range between the edge and top of the melting peak.

RESULTS

Reaction Of 1 With *p*-quinones

Upon mixing **1** and *p*-benzoquinone (BQ), the solution immediately changed from colorless to yellow. The products were identified as monoimine (**2**), diimine (**3**), and hydroquinone, whereas *p*-BQ was almost completely reacted. The stoichiometric balance was kept among all the products and the starting materials. Figure 2

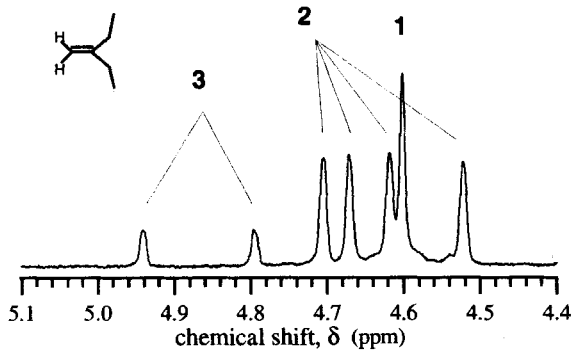

FIGURE 2 ^{1}H NMR spectrum (in DMSO-d_6) for the reaction of **1** and *p*-BQ. The olefinic peaks are assigned to the exomethylene protons of **1**, **2**, and **3**.

shows the exomethylene region ^{1}H NMR spectrum for the reaction mixture (1.0 eq. of quinone), where seven olefinic peaks were assigned as follows: δ 4.60–**1**, δ 4.52, 4.61, 4.67 and 4.70–**2**, δ 4.80 and 4.94–**3**, respectively. The chemical structures of **2** and **3** were deduced from two-dimensional NMR measurements including COSY, NOESY, and HMQC: for **3**, two distinct exomethylene protons are attached to the same carbon. It is noteworthy that only two of the four benzylamine moieties are *regioselectively* oxidized, leading to a "diagonal" diimine. Any other regioisomers of **3** could not be found.

Depending on the initial molar ratio of quinone, the resultant molar contents of the products were changed. Figure 3 shows the molar content of each component that was evaluated from the peak areas of their ^{1}H NMR signals. This figure clearly shows that **1** reacts with two equivalents of *p*-BQ almost quantitatively in the two-step manner. The reaction scheme can be represented by Eqs. (1) and (2), which show that one quinone molecule (Q) is converted to hydroquinone (QH2), while one benzylamino moiety reacts to form benzylideneamine.

$$1 + Q \rightarrow 2 + QH_2 \quad (1)$$

$$2 + Q \rightarrow 3 + QH_2 \quad (2)$$

A similar experiment using chloranail (TCBQ) instead of *p*-BQ gave essentially an identical

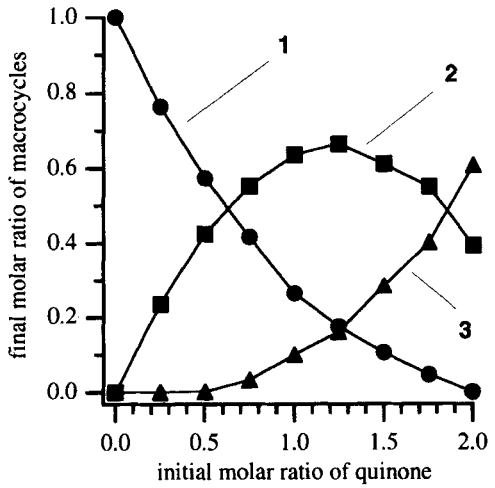

FIGURE 3 Molar ratios of **1**, **2** and **3** as functions of initial molar ratio of *p*-BQ.

result (data not shown). As for **4a–c**, their reactions with quinones afforded only monoimine compounds, indicating that the reaction basically follows Eq. (1). For **4d** and **e**, similar reactions were not observed.

Kinetic Analyses for the Reaction

In Fig. 3, each curve is a function of the ratio of the observed rate constants for Eq. (1) (k_{obs1}) to that for Eq. (2) (k_{obs2}). By comparison with a theoretical simulation, k_{obs1} and k_{obs2} was estimated at ~5 for both the cases of *p*-BQ and chloranil. We attempted more precise determination of k_{obs1} and k_{obs2} by UV–Vis measurement, but the difference in absorption maximum between **2** and **3** is too small to separate the contribution from each constant. Therefore, we focused on k_{obs1}, and this paper denote it simply as k_{obs}. After addition of 0.2 equivalents of quinone for **1**, the absorbance at 379 nm was monitored to follow the reaction. As can be seen in Fig. 3, the generation of **3** is negligible under this condition. Neither absorptions of quinones nor hydroquinones affect the monitoring region.

The value of k_{obs} for several *p*-quinones (chloranil, bromanil (TBBQ), 2,5-dichloro-*p*-benzoquinone (DCBQ), 2-chloro-*p*-benzoquinone

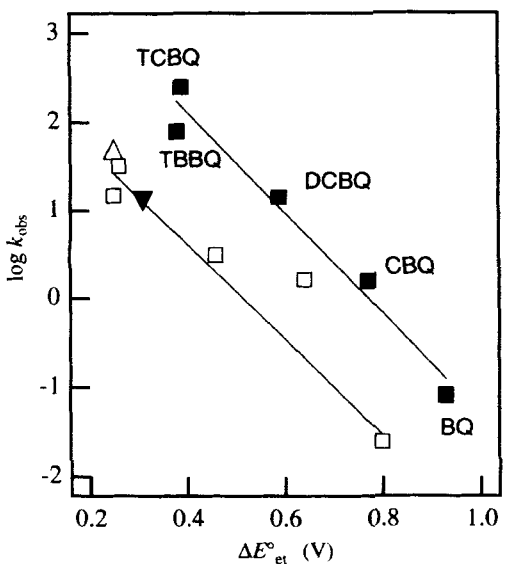

FIGURE 4 The values of $\log k_{obs}$ (K_{obs} are measured in $M^{-1}s^{-1}$) for **1** (■) and **4a** (□) as a function of ΔE^0_{et} (for definition, see text). The abbreviations of *p*-quinones are attached to the symbol (■). In the linear regression analysis of **4a**, data for CBQ was removed. Data for the reaction of **4b**(Δ) and**4c** (▼) with chloranil are also shown.

(CBQ), *p*-BQ, 2,5-dimethyl-*p*-benzoquinone (DMBQ), 2,3,5,6-tetramethyl-*p*-benzoquinone, 1-4-napthoquinone, anthraquinone and 2,3-dimethoxy-5-methyl-*p*-benzoquinone) were measured. For TCBQ, TBBQ, DCBQ, CBQ and BQ, the time dependent changes of the absorbance were successfully analyzed by assuming second order reaction. As for the other quinones used, the reaction rates were too small to be accurately determined.

Figure 4 plots the values of $\log k_{obs}$ against the difference in redox potentials (ΔE^0_{et}) between **1** and *p*-quinone (i.e., $\Delta E^0_{et} = E^0_{OX} - E^0_{red}$, where E^0_{OX} and E^0_{red} are $E_{1/2}$ of one-electron redox wave of **1** to *p*-quinone, respectively). There is a linear relation between $\log k_{obs}$ and ΔE_{et}, clearly indicating that the reaction rate is governed by one-electron transfer from **1** to *p*-quinone. However, when, 7,7,8,8-tetracyanoquinodimethane (TCNQ) was used instead of *p*-quinone, increase in absorbance at 379 nm was observed, although its one-electron redox potential (−0.10 V) is more positive than that of chloranil (−0.35 V). This implies that the initial stage of this reaction involves some interactions related to the subsequent proton transfer process.

Similarly, the rate constant for **4a–c** were measured. As can be seen in Fig. 4, the ΔE^0_{et} dependence of k_{obs} for **4a** is similar to that of **1**, accompanied by an appreciable shift of the intercept. Each regression line **1** and **4a** is expressed by Eqs. (3) and (4), respectively.

$$\log k_{obs} = -5.7\,\Delta E^0_{et} + 4.4 \quad (3)$$

$$\log k_{obs} = -5.4\Delta E^0_{et} + 2.8 \quad (4)$$

where ΔE^0_{et} is measured in volts. The k_{obs} values of **4b** and **4c** with chloranil are superimposed in Fig. 4. They appear to follow Eq. (4), indicating that the difference in rate constants among **4a–c** arises from their differences in redox potential.

On the other hand, **4d** and **4e** did not react with *p*-quinones in the same manner as **4a**. Although the redox potential **4d** and **4e** (+0.18 and +0.16 V, respectively) are more positive than that of **4a** (−0.10 V), their inactivity is not completely explained from the difference in redox potential.

Electrochemical Study on the Reaction System

Cyclic voltammograms were successfully obtained for each compound. For **4a–e**, however, irreversible reduction waves were observed after two-electron oxidation. Thus, we took the sweep region so that only one-electron redox reaction could occur. The one-electron redox potentials of

TABLE I The one-electron redox potentials of the compounds studied (in V vs Ag^+/Ag).

Compound	E_{anodic}	$E_{cathodic}$	$E_{1/2}$
1	+0.13	−0.15	−0.01
4a	+0.02	−0.21	−0.10
4b	+0.02	−0.23	−0.11
4c	+0.08	−0.15	−0.04
4d	+0.27	+0.09	+0.18
4e	+0.35	−0.03	+0.16
p-Phenylenediamide	+0.10	−0.22	−0.06

the compounds studied are summarized in Table I. Figure 5(a) shows the voltammogram of **1**.

To examine the interaction between **1** and *p*-quinone, the voltammograms were measured for the system composed of **1** and DMBQ. Since the redox potential of DMBQ (−1.10 V) is so negative that the reactions shown in Eqs. (1) and (2) is negligible during the measuring period. Figure 5(a) shows the voltammogram of DMBQ in the region of a one-electron redox reaction. As shown in Fig. 5(b), upon incremental addition of 2.0 equivalents of **1** to the solution of DMBQ (1.0 mM), two peaks gradually appeared around −0.3 V (anodic) and −0.7 V (cathodic) together with a decrease of anodic peak at −0.96 V that corresponds to $Q^{\cdot-} \rightarrow Q$ process. In addition, the cathodic peak current at −1.2 V slightly increases with increasing amount of **1**.

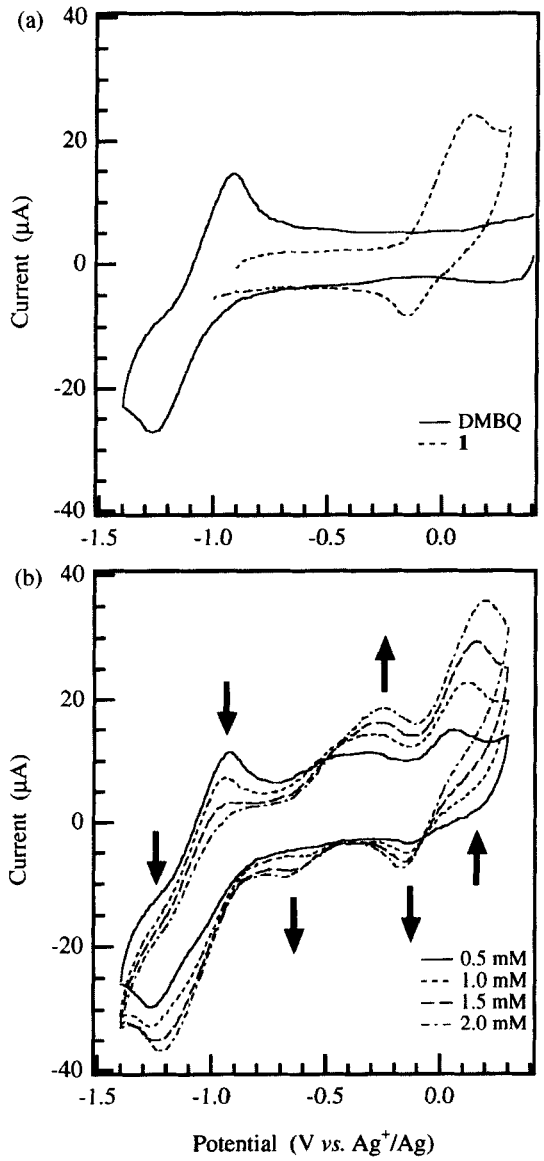

FIGURE 5 Cyclic voltammograms of 1 and DMBQ: (a) results for individual measurement, and (b) results for an incremental addition of 1 to DMBQ.

Similar changes in redox wave have been observed for *p*-quinones in the presence of strong hydrogen-bonding reagent such as hexafluoro-2-propanol (HFIP) [17]. In such a system, by addition of HFIP, a new anodic peak corresponding to the oxidation of hydrogen-bonded quinone appears at about 1.0 V on the positive side of the original $Q^{\cdot-} \rightarrow Q$ peak. This accompanies a decrease of the $Q^{\cdot-} \rightarrow Q$ peak current. In addition, a new cathodic peak that corresponds to the reduction of hydrogen-bonded quinone appears prior to the original $Q \rightarrow Q^{\cdot-}$ peak. This is followed by disproportionation processes, leading to an apparent increase of the $Q \rightarrow Q^{\cdot-}$ peak current. Such a change in the redox potential due to hydrogen bonding is supported by theoretical calculation [18].

The above interpretation can be applied to the present case. A similar phenomenon was also observed for **4a**, but not for *p*-phenylenediamine, indicating that the phenolic OH groups are concerned with the hydrogen bonding. The peak at −0.3 V does not appear when sweeping between −0.80 V and +0.30 V, whereas the peak at −0.7 V does not appear when sweeping between −1.40 V and −0.20 V. When sweeping between −0.8 V and −0.2 V,

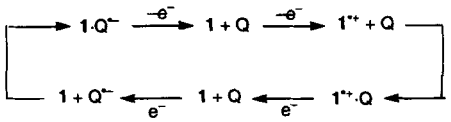

SCHEME 1

neither peaks were observed. These results implies that the new peaks originate from transient spices composed of a radical ion and a neutral molecule as shown in Scheme 1: the peaks at −0.3 V and −0.7 V can be assigned to the oxidation of $\mathbf{1}\cdot Q^{\cdot-}$ and the reduction of $1^{\cdot+}Q$, respectively. The latter is also supported by a relatively small increase in cathodic current at −0.2 V in comparison with an increase in anodic current at + 0.2 V. Consequently, by means of hydrogen bonding with OH groups, **1** or **4a–c** can interact with quinone, resulting in positive shift of the redox potential of the quinone. Such an activation of quinone is also observed for Hunter's quinone receptor [19].

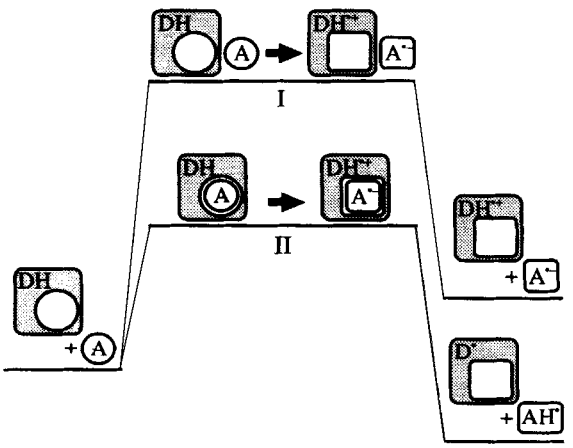

FIGURE 6 Schematic representation of an electron transfer reaction from a macrocyclic donor with proton source (DH) to an acceptor (A). If the reduced state of A is stabilized by the complexation with the oxidized state of DH, the activation energy of a complexed form (II) is decreased compared with that of an uncomplexed form (I).

DISCUSSION

It is worth noting that the reduction of *p*-quinone by **1** is apparently accelerated in comparison with that by its acyclic analogues, although the reaction itself is rather likely from the viewpoint of the oxidation of an aromatic amine.

The linear relation between $\log k_{obs}$ and ΔE^0_{et} (Fig. 4) shows the rate determining step is related to the one-electron transfer process. From a simple consideration based on the redox potentials of **1** and *p*-BQ, the free energy change ($\Delta G_{et} = F\,\Delta E^0_{et}$, where F is Faraday constant) reaches 90 kJ mol^{-1} which corresponds to a bimolecular reaction rate constant of $\sim 10^{-3}$ M^{-1} s^{-1} at most. The rate constant actually observed for *p*-BQ is 0.08 M^{-1} s^{-1}, which is much larger than expected. Such acceleration may be caused by hydrogen bonding between quinone and **1**. The electrochemical measurements showed that the presence of **1** and quinone induces a sizable shift of the redox potential in each species. Namely, the redox potential of $\mathbf{1}^{\cdot+}\cdot Q/\mathbf{1}\cdot Q^{\cdot-}$ is more positive than that of $Q/Q^{\cdot-}$, whereas the redox potential of $\mathbf{1}^{\cdot+}\cdot Q/\mathbf{1}\cdot Q$ is more negative than that of $\mathbf{1}^{\cdot+}/\mathbf{1}$. Therefore, through complexation, an apparent Gibbs energy change becomes less than $F\Delta E^0_{et}$ to some extent. Here we define ΔG_{HB} (<0) as the Gibbs energy change caused by the hydrogen bonding between **1** and quinone. Thus, the Gibbs energy change for electron transfer (ΔG_{et}) is written by Eq. (5)

$$\Delta G_{et} = F\Delta E^0_{et} + \Delta G_{HB} \qquad (5)$$

The strength of the hydrogen bond depends on the basicity of quinones. On considering pH dependence of the one-electron reduction potential of quinones [5], we can presume that the magnitude of ΔG_{HB} increases in the order of TBBQ ≈ TCBQ < DCBQ < CBQ < BQ < DMBQ. This assumption can explain why the slope ($-5.7\,V^{-1}$) in Fig. 4 is relatively gentle to the corresponding coefficient ($-14.4\,V^{-1}$) obtained for an NADH model compound [5].

Based on the above consideration, the pathway to the one-electron transfer involves the complexation of **1** and quinone, which plays a role not only in lowering the activation barrier but also in making the donor and acceptor approach each other so that an efficient electron transfer could occur. If we assume such complexation, the reaction coordinate can be schematically shown

in Fig. 6, where the apparent rate constant k_{obs} is the product of the equilibrium constant of the complex (K_{comp}) and the rate constant of electron transfer (k_{et}), that is, $k_{obs} = K_{comp}k_{et}$. On comparing this figure with Fig. 1, one can see that **1** acts as if a catalyst were present in the system.

According to the Marcus theory [20], the rate constant (k_{et}) of electron transfer is determined by the free energy change of electron transfer (ΔG_{et}) and the reorganization energy associated with the electron transfer (λ).

$$\log k_{et} \propto \frac{\lambda}{4}\left(1 + \frac{\Delta G_{et}}{\lambda}\right)^2 \qquad (6)$$

We adopt an approximation by which the second-order term with respect to ΔG is neglected, based on the fact that $\log k_{obs}$ is in proportion on ΔE^0_{et} (Eqs. (3) and (4)). Then, from Eqs. (5) and (6), k_{obs} is expressed as follows:

$$\log k_{obs} = \log (K_{comp}k_{et})$$

$$= K(\Delta G_{comp} + F\Delta E^0_{et} + \Delta G_{HB}) + C \qquad (7)$$

Where ΔG_{comp} includes the Gibbs energy necessary for the quinone and the reductant (**1** or **4a–c**) to approach each other and the reorganization energy of solvents, and K and C are constants.

Here we analyze Eqs.(3) and (4) on the basis of Eq. 7. Because ΔG_{HB} is a term predominantly dependent on the nature of quinone, the difference in coefficients between Eqs. (3) and (4) is attributed to the ΔG_{comp} term. Substituting Eqs. (3) and (4) in Eq. 7 gives the difference ($-27\,kJ\,mol^{-1}$) in ΔG_{comp} between **1** ($\Delta G_{comp(1)}$) and **4a** ($\Delta G_{comp(4a)}$).

$$\Delta G_{comp(1)} - \Delta G_{comp} = -27\,kJ\,mol^{-1} \qquad (8)$$

In analogy with the cases of crown ether and many other inclusion compounds, the main part of $-27\,kJ\,mol^{-1}$ can be interpreted from entropic effect on complexation [14,15]. This value is comparable to the difference in Gibbs change ($25\,kJ\,mol^{-1}$) for complexation with potassium ion on going from pentaethylene glycol dimethyl ether to [18]crown-6. This corresponds to 10^4-fold difference in stability for the complex. For **1**, its 34-membered ring is a reasonable size to specifically interact with *p*-quinones as compared with several quinone receptors reported so far [21–23].

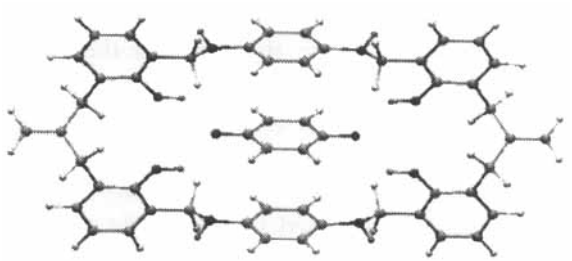

FIGURE 7 A possible structure of the **1**-quinone complex, obtained by molecular mechanics calculation with AMBER* force field. The program is packaged in MacroModel® [24].

Figure 7 depicts a possible structure of the **1**-quinone complex that was obtained as a significantly stable conformer by molecular mechanics calculations (AMBER* force field). For this structure, the average distance OH···O between **1** and quinone is 1.89Å, which is within a range for typical hydrogen bonds. The *p*-phenylene rings of **1** and the molecular plane of quinone are almost parallel to each other, and the interplane distance is 3.34Å, which is within a range for typical $\pi-\pi$ stacking structures. It is expected from this structure that the four OH groups of **1** and two C=O groups of *p*-quinone form a hydrogen bond network, making an enthalpic contribution to the formation of the **1**-quinone complex at the first stage of the reaction. The $\pi-\pi$ stacking structure might contribute to stabilizing the complex, and simultaneously aid the effective electron transfer from **1** to *p*-quinone. The importance of the spatial arrangement of OH groups was also shown by the results for the **4a**, **4d** and **4e**: *o*- (**4d**) and *m*- (**4e**) isomers which exhibit quite a lower reactivity against quinones than expected from their $E_{1/2}$ value.

It is still not obvious why the final oxidation product of **1** is the "diagonal" diimine (**3**). First, we consider why the reaction of **4a** with quinone stops

at the formation of the monoimine compound. This is explained from the fact that the donor ability of aniline is increased by an electron donating substituent at the *p*-position: after one side of benzylamino group of **4a** is converted to benzylimino group, the reactivity of the other side is considerably decreased. Consequently, after one benzylamino group of **1** is oxidized, there are two reactable sites remaining. At this stage, namely for **2**, the NMR signal of the hydroxy group of the –Ar(OH)–CH=N– moiety appears at the extremely lowfield region (14.09 ppm in DMSO-d_6), indicating a strong intramolecular hydrogen bond making pseudo six-membered ring. Such a strong hydrogen bond may bring about a drastic change in conformation, resulting in definitive differences in the reactivity among the benzylamino groups.

In conclusion, we have found that a macrocyclic compound **1** has the ability to reduce *p*-quinones into the corresponding hydroquinone almost quantitatively. By comparison with its acyclic analogues, the macrocyclic effect on the reaction rate was clearly observed. The rate determining step involves a one-electron transfer from **1** to quinone. Prior to the electron transfer, **1** and quinone form a transient complex. As the difference in Gibbs energy necessary for the complexation, we estimated the macrocyclic effect to be $-27\,\mathrm{kJ\,mol^{-1}}$. In this complex, four hydroxy groups of **1** are effectively arranged so that the donor and acceptor sufficiently approach each other. Upon complexation, by hydrogen bonding the redox potentials of **1** and *p*-quinone are shifted to the negative and positive side, respectively, leading to lowering of the activation barrier of electron transfer. Consequently, **1** is a donor reagent as well as a molecular host, which acts as if a catalyst were present in the system. In other words, this macrocyclic compound promotes its own reactivity by the aid of its macrocyclic structure. In this regard, it can be said that this is a new example of the macrocyclic effects.

References

[1] Kurreck, H. and Huber, M. (1995), *Angew. Chem. Int. Ed. Engl.* **34**, 849.
[2] Sessler, J.L., Wang, B. and Harriman, A. (1993), *J. Am. Chem. Soc.* **115**, 10418.
[3] Hunter, C.A. and Shannon, R.J. (1996), *Chem. Commun.*, 1361.
[4] Fukuzumi, S., Komitsu, S., Hironaka, K. and Tanaka, T. (1987), *J. Am. Chem. Soc.*, **109**, 305.
[5] Fuzukumi, S., Ishikawa, M. and Tanaka, T. (1989), *J.Chem, Soc., Perkin Trans. 2*, 1181.
[6] Ishikawa, M., Matsuda, Y., Yamamoto, K. and Fuzukumi, S. (1992), *Chem. Lett.*, 2269.
[7] Coleman, C., Rose, J. and Murray, C. (1992), *J. Am. Chem. Soc.* **114**, 9755.
[8] Hubig, S. and Kochi, J. (1999), *J. Am. Chem. Soc.* **121**, 1688.
[9] Zaman, K., Yamamoto, S., Nishimura, N., Murata, J. and Fukuzumi, S. (1994), *J. Am. Chem. Soc.* **116**, 12099.
[10] Fukuzumi, S. (1997), *Bull. Chem. Soc. Jpn.* **70**, 1.
[11] Laviron, E. (1986), *J. Electroanal. Chem.* **208**, 357.
[12] Hayashi, T., Miyahara, T., Aoyama, Y., Nonoguchi, M. and Ogoshi, M.H. (1994), *Chem. Lett.*, 1749.
[13] D'Souza, F. (1996), *J. Am. Chem. Soc.* **118**, 923.
[14] Voegtle, F. (1993) *Supramolecular Chemistry: An Introduction* (Wiley, Chichester).
[15] Lehn, J.-M. (1995) *Supramolecular Chemistry: Concepts and perspectives* (VCH, Weinheim).
[16] Houjou, H., Lee, S.-K., Hishikawa, Y., Nagawa, Y. and Hiratani, K. (2000), *Chem. Commun.*, 2197.
[17] Gupta, N. and Linschitz, H. (1997), *J. Am. Chem. Soc.* **119**, 6384.
[18] O'Malley, P.J. (1997), *Chem. Phys. Lett.* **274**, 251.
[19] Brooksby, P.A., Hunter, C.A., Mcquillan, A.J., Purvis, D.H., Rowan, A.E., Shannon, R.J. and Walsh, R. (1994), *Angew. Chem. Int. Ed. Engl.* **33**, 2489.
[20] Marcus, R.A. (1964), *Annu. Rev. Phys. Chem.* **15**, 155.
[21] Aoyama, Y., Asakawa, M., Matsui, Y. and Ogoshi, H. (1991), *J. Am. Chem. Soc.* **113**, 6233.
[22] Hunter, C.A. (1991), *J. Chem. Soc. Chem. Commun.*, 749.
[23] Tanaka, K., Yamamoto, Y., Machida, I. and Iwata, S. (1999), *J.Chem. Soc., Perkin Trans. 2*, 285.
[24] Mohamadi, F., Richards, N.G.J., Guida, W.C., Liskamp, R., Lipton, M., Caufield, C., Chang, G., Hendrickson, T. and Still, W.C. (1990), *Comput. Chem.* **11**, 440.